SIAM J. APPL. MATH.
Vol. 78, No. 1, pp. 63–79

FROM TRAFFIC AND PEDESTRIAN FOLLOW-THE-LEADER MODELS WITH REACTION TIME TO FIRST ORDER CONVECTION-DIFFUSION FLOW MODELS*

ANTOINE TORDEUX†, GUILLAUME COSTESEQUE‡, MICHAEL HERTY§, AND ARMIN SEYFRIED†

Abstract. In this work, we derive first order continuum traffic flow models from a microscopic delayed follow-the-leader model. These are applicable in the context of vehicular traffic flow as well as pedestrian traffic flow. The microscopic model is based on an *optimal* velocity function and a reaction time parameter. The corresponding macroscopic formulations in Eulerian or Lagrangian coordinates result in first order convection-diffusion equations. More precisely, the convection is described by the optimal velocity while the diffusion term depends on the reaction time. A linear stability analysis for homogeneous solutions of both continuous and discrete models is provided. The conditions match those of the car-following model for specific values of the space discretization. The behavior of the novel model is illustrated thanks to numerical simulations. Transitions to collision-free self-sustained stop-and-go dynamics are obtained if the reaction time is sufficiently large. The results show that the dynamics of the microscopic model can be well captured by the macroscopic equations. For nonzero reaction times we observe a scattered fundamental diagram. The scattering width is compared to real pedestrian and road traffic data.

Key words. first order traffic flow models, micro/macro connection, hyperbolic conservation laws, Godunov scheme, numerical simulation

AMS subject classifications. 35F20, 70F45, 90B20, 65M12

DOI. 10.1137/16M110695X

1. Introduction.

Microscopic and macroscopic approaches for the purpose of vehicular traffic flow modeling have often been developed separately in the engineering community [44, 23, 5, 26]. Similar models can also be used in the description of pedestrian dynamics [41, 11, 1]. Typically, microscopic models are based on the so-called *follow-the-leader* strategy, and they are stated as (finite or infinite) systems of ordinary differential equations (ODEs). They are generally based on speed or acceleration functions which depend on distance spacing, speed, predecessor speed, relative speed, and so on. One of the simplest approaches is a speed model solely based on the spacing, first proposed by Pipes [39],

$$\dot{x}_i(t) = W(\Delta x_i(t)), \tag{1}$$

where $\Delta x_i(t) = x_{i+1}(t) - x_i(t)$ denotes the spacing between the vehicle (i) and its predecessor $(i+1)$ and $W(\cdot)$ stands for the equilibrium (or optimal) speed function depending on the spacing. The microscopic models are discrete in the sense that the vehicles or pedestrians $i \in \mathbb{Z}$ are individually considered. A macroscopic description considers the flow of vehicles or pedestrians (in the following also referred to as *agents*)

*Received by the editors December 12, 2016; accepted for publication (in revised form) November 15, 2017; published electronically January 5, 2018.
http://www.siam.org/journals/siap/78-1/M110695.html

†Forschungszentrum Jülich GmbH and Bergische Universität Wuppertal, Wuppertal, Germany (a.tordeux@fz-juelich.de, a.seyfried@fz-juelich.de).

‡INRIA Sophia Antipolis–Méditerranée, Sophia Antipolis, Valbonne, France (guillaume.costeseque@inria.fr).

§Rheinisch–Westfälische Technische Hochschule Aachen, Aachen D-52056, Germany (herty@igpm.rwth-aachen.de).

as a continuum in Eulerian or Lagrangian coordinates. For instance, in the most classical Eulerian time-space framework, the main variables are the density, the flow, and the mean speed. The simplest approach is the scalar hyperbolic equation of the celebrated Lighthill–Whitham–Richards (LWR) model [30, 40]

$$\partial_t \rho + \partial_x(\rho V(\rho)) = 0. \tag{2}$$

Here ρ is the density, and $V(\cdot)$ is the equilibrium speed function which is assumed to depend only on the density. The flow $Q(\rho) = \rho V(\rho)$ is given by the product of the density times the mean speed. The model is derived from the continuity equation for which the flow is supposed in equilibrium. The microscopic and macroscopic models (1) and (2) well reproduce shock-wave phenomena for Riemann problems. Yet such models are not able to describe the observed transition to scattered flow/density relation (the fundamental diagram) with hysteresis and self-sustained stop-and-go phenomena (see [45, 25, 10], [24, Figure 1], [49, Figure 5], and Figures 8 and 9). This is due to the fact that spatially homogeneous regimes are always in the equilibrium solutions and are determined by the functions $W(\cdot)$ and $V(\cdot)$, respectively.

Therefore, the microscopic behavior is modified by introducing reaction and relaxation times. The simplest car-following model of this type may be the delayed model by Newell [32]

$$\dot{x}_i(t+\tau) = W(\Delta x_i(t)), \tag{3}$$

with τ the reaction time (if positive). Applying a Taylor expansion in the left-hand side of the delayed speed model (3), we obtain the second order "optimal velocity model" (OVM) introduced by Bando et al. in [4]. The OVM has limit-cycles in stationary states, with self-sustained propagation of nonlinear stop-and-go waves, and hysteresis curves in the fundamental flow/density diagram (see [35, 36]). Macroscopic second-order models comprised of systems of hyperbolic equations are also able to reproduce nonlinear stop-and-go waves and scattering of the fundamental diagram. One of the first approaches is that of Payne and Whitham (PW) [38, 47]. The model can be derived from the microscopic Newell model (3). The main drawback of this model is that, as pointed out by Daganzo [14], the speed and density could yield negative values and are not bounded. Note that this drawback is also observed with follow-the-leader models like the OVM and is referred to as collision between the vehicles (see, for instance, [15, 37] or [44, Chap. 15]). Aw and Rascle have corrected this issue by replacing the space derivative of the "pressure" by a convective derivative [3] (AR model). Today extensions of the AR model, such as the ARZ, GARZ, or generalized models [22, 48, 6, 18, 42, 17], as well as two phase models coupled with the LWR model [12, 20, 13, 7], are used to describe transition to congested traffic with scattered fundamental diagrams and self-sustained nonlinear shock waves. A general framework is the generic second order model (GSOM) family introduced in [29, 28]. Most of the approaches are a posteriori based on the continuous description.

In this article, we derive minimalist macroscopic traffic flow models of first order from a microscopic speed model to describe stop-and-go wave phenomena and scattering of the fundamental diagram. The use of first order models allows us to ensure by construction that the speed and density remain positive and bounded. The starting point is an optimal velocity microscopic model of first order including a reaction time parameter. We show in section 2 that the corresponding macroscopic model results in a convection-diffusion equation. The macroscopic model is discretized using distinct Godunov and Euler-based schemes, and the linear stability conditions for the

homogeneous solutions of these numerical schemes are provided in section 3. The conditions match those of the car-following model for specific values of the spatial discretization step. Simulations are carried out in section 4. Systems with different initial conditions are numerically solved. Further, we compare the model to real data of traffic as well as pedestrian flows.

2. Microscopic and macroscopic models.

2.1. The microscopic follow-the-leader model. The microscopic model we use has been introduced in [43]. It is based on the Newell model (3). In the remainder of the paper, we assume that $W : s \mapsto W(s)$ is Lipschitz continuous, nondecreasing, and upper-bounded in order to get the well-posedness of (3) supplemented with initial conditions $x_i(t = 0) = x_{i,0}$ for any $i \in \mathbb{Z}$. We rewrite the equation as

$$\dot{x}_i(t) = W(x_{i+1}(t - \tau) - x_i(t - \tau)) \tag{4}$$

and apply a Taylor expansion in the argument of W. Neglecting higher-order terms in τ, we obtain

$$\dot{x}_i(t) = W\big(\Delta x_i(t) - \tau\big[W(\Delta x_{i+1}(t)) - W(\Delta x_i(t))\big]\big). \tag{5}$$

The model is a system of ODEs of first order with two predecessors in interaction. It is calibrated by the delayed time $\tau \in \mathbb{R}$, that is, a reaction time if positive and an anticipation time if negative, and the optimal speed function $W(\cdot)$. The function $W(\cdot)$ is supposed to be bounded by $V_0 > 0$, positive, and zero if the spacing is smaller than ℓ, $\ell > 0$ being the vehicle's length or size of the pedestrian. Note that the model admits a minimum principle, say $\Delta x_i(t) \geq \ell$ for all i, t. Thus it is by construction collision-free, and it has the same stability condition as the initial microscopic Newell model (3) or as the OVM from [4]. This condition is for all $s \in \mathbb{R}$

$$|\tau| W'(s) < 1/2. \tag{6}$$

Note that the condition simply reduces to $|\tau| < T/2$ if one considers the linear fundamental diagram $W : s \mapsto W(s) := \max\big\{0, \min\big\{\frac{1}{T}(s - \ell), V_0\big\}\big\}$, with $T > 0$. When unstable, the model transitions to states with collision-free self-sustained stop-and-go dynamics; see [43].

2.2. Derivation of macroscopic models. In the following, we consider $i = 1, \ldots, N$ agents with periodic boundary conditions (i.e., the predecessor of the agent N is the agent 1). The derivation of macroscopic models from microscopic models is useful to fully understand the dynamics. In [2], Aw et al. established the connection between a microscopic car-following model and the second order AR macroscopic traffic flow model. The rigorous proof, based on a scaling limit where the time and space linearly increase while the speed and the density remain constant, assumes homogeneous conditions. We use here the same methodology considering the local density $\rho_i(t)$ around the vehicle or pedestrian (i) and at time $t > 0$, as the inverse of the spacing

$$\rho_i(t) := \frac{1}{\Delta x_i(t)}. \tag{7}$$

The density could also be normalized by multiplication with ℓ. Here, we prefer to keep the unit of one over length as density to ease the comparison with the classical

models. Then, the microscopic model reads

$$\dot{x}_i(t) = W\left(\frac{1}{\rho_i(t)} - \tau\left[W\left(\frac{1}{\rho_{i+1}(t)}\right) - W\left(\frac{1}{\rho_i(t)}\right)\right]\right) =: \tilde{V}(\rho_{i+1}(t), \rho_i(t)) \tag{8}$$

for a velocity profile $\tilde{V}$. Then,

$$\partial_t \frac{1}{\rho_i(t)} = \partial_t \Delta x_i(t) = \tilde{V}(\rho_{i+2}(t), \rho_{i+1}(t)) - \tilde{V}(\rho_{i+1}(t), \rho_i(t)). \tag{9}$$

In [2] it has been observed that (9) is a semidiscretized version of a hyperbolic partial differential equation in Lagrangian coordinates. This requires us to consider limits of many vehicles or pedestrians $N \to \infty$ and diminishing length $\ell \to 0$. We introduce the continuous variable $y \in \mathbb{R}$ such that $y_i = i\Delta y$ as a counting variable for the number of agents where Δy is proportional to ℓ. By piecewise constant extension of the given spacing, we construct a density $\rho(t, y)$ such that $\frac{1}{\rho_i(t)} = \frac{1}{\Delta y}\int_{y_i - \frac{\Delta y}{2}}^{y_i + \frac{\Delta y}{2}} \frac{1}{\rho(t,z)} dz$. The quantity $\frac{1}{\rho_i(t)}$ is the volume average over a cell of length Δy centered at y_i. The right-hand side of (9) describes the flux across the cell boundaries. Introduce $V : k \mapsto V(k) = W(\frac{1}{k})$ for any $k > 0$. Then, it follows that $\tilde{V}(k_1, k_2) = V(\frac{k_2}{1 - k_2\tau[V(k_1) - V(k_2)]})$ for any $(k_1, k_2) \in (0, +\infty)^2$ satisfying $V(k_1) \neq V(k_2) + \frac{1}{\tau k_2}$. As for OVM, W is nondecreasing; therefore, we observe that V is nonincreasing on $(0, +\infty)$. We obtain from (9)

$$\partial_t \frac{1}{\rho_i(t)} - \frac{\Delta y}{\Delta y}\left[V\left(\frac{\rho_{i+1}}{1 - \tau\rho_{i+1}Z_{i+1}}\right) - V\left(\frac{\rho_i}{1 - \tau\rho_i Z_i}\right)\right] = 0, \tag{10}$$

where $Z_i := V(\rho_{i+1}) - V(\rho_i)$. Provided that $-V$ is increasing and $\rho(t, y)$ is piecewise constant on each cell, the reconstruction at the cell interface $y_{i\pm\frac{1}{2}}$ is given by cell averages, i.e., $\frac{1}{\rho(t, y_{i+\frac{1}{2}})} = \frac{1}{\rho_{i+1}(t)}$. Next, we rescale time $t \to t\Delta y$ and also reaction time $\tau \to \tau\Delta y$ to obtain

$$\partial_t \frac{1}{\rho_i(t)} - \frac{1}{\Delta y}\left[V\left(\frac{\rho_{i+1}}{1 - \tau\rho_{i+1}\frac{Z_{i+1}}{\Delta y}}\right) - V\left(\frac{\rho_i}{1 - \tau\rho_i\frac{Z_i}{\Delta y}}\right)\right] = 0. \tag{11}$$

Hence, we observe that in the rescaled time and in the limit $\Delta y \to 0$ the microscopic model is an upwind discretization of the following macroscopic equation:

$$\partial_t \frac{1}{\rho} - \partial_y V\left(\frac{\rho}{1 - \tau\rho\partial_y V(\rho)}\right) = 0. \tag{12}$$

The upwind or Godunov scheme is the most mathematically reasonable discretization provided τ is sufficiently small due to the decreasing behavior of V for suitable OVM functions W. Up to second order in τ we approximate (12) by Taylor expansion and obtain a convection-diffusion model such as

$$\partial_t \frac{1}{\rho} - \partial_y V(\rho) = \tau\partial_y\big((\rho V'(\rho))^2 \partial_y \rho\big). \tag{13}$$

The relation between the density in Lagrangian coordinates and Eulerian coordinates is given by the coordinate transformation $(t, y) \to (t, x)$ where $y = \int_{-\infty}^{x} \rho(t, x) dx$.

Note that y counts the number of vehicles/pedestrians up to position x in Eulerian coordinates. In the Eulerian coordinates (t, x), the macroscopic model (12) reads

$$\partial_t \rho + \partial_x \left(\rho V \left(\frac{\rho}{1 - \tau \partial_x V(\rho)} \right) \right) = 0. \tag{14}$$

The model could be seen as an extension of the LWR model (2) with a modified speed-density relationship $\rho \mapsto V\left(\rho/(1 - \tau \partial_x V(\rho))\right)$. Such a family of models is related to fictitious density nonlinear diffusion models in the literature [8]. For illustrating the behavior of this modified speed-density mapping, we set $I := \tau \partial_x V(\rho))$, and we define $\mathcal{V} : (\rho, I) \mapsto V\left(\rho/(1 - I)\right)$. The fundamental diagrams obtained for a constant term $I \in \{-0.3, 0, 0.3\}$ and for a speed function $V : \rho \mapsto \max\{0, \min\{2, 1/\rho - 1\}\}$ are shown in Figure 1. Note that for constant (in space) densities ρ (and/or for $\tau = 0$), the additional term I vanishes, and we recover the classical LWR model.

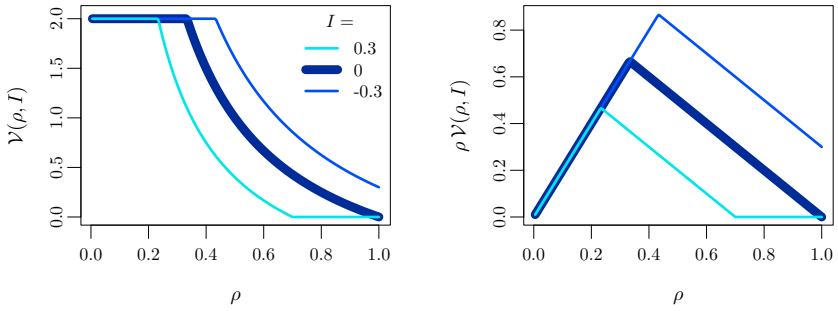

FIG. 1. *Illustration for the fundamental diagram* $\mathcal{V} : (\rho, I) \mapsto V\big(\rho/(1 - I)\big)$ *obtained in the macroscopic model* (14) *with constant inhomogeneity* $I \in \{-0.3, 0, 0.3\}$ *and* $V : \rho \mapsto \max\{0, \min\{2, 1/\rho - 1\}\}$.

A Taylor expansion up to second order in terms of τ for (14) yields

$$\partial_t \rho + \partial_x(\rho V(\rho)) = -\tau \partial_x \left((\rho V'(\rho))^2 \partial_x \rho \right). \tag{15}$$

We also consider an initial condition

$$\rho(t = 0, x) = \rho_0(x) \quad \text{for any} \quad x \in \mathbb{R}, \tag{16}$$

where $\rho_0 \in L^1(\mathbb{R}) \cap \mathrm{BV}(\mathbb{R})$. Equation (15) is a partial differential equation of the first order in time and of the second in space. Oppositely to classical second order approaches such as PW, AR, ARZ, and GSOM models [38, 47, 3, 48, 28] which are hyperbolic, the model is parabolic and simply requires Neumann boundary conditions.

By defining $D(\rho) := \int_{-\infty}^{x} -\tau(\rho V'(\rho))^2 \partial_x \rho \, \mathrm{d}y$, we obtain a diffusion equation similar to the one considered in [9], say

$$\partial_t \rho + \partial_x(\rho V(\rho)) = \partial_x^2 D(\rho). \tag{17}$$

One can verify that $D(\rho_0)$ is absolutely continuous on $\mathbb{R}$ and that $\partial_x D(\rho_0) \in \mathrm{BV}(\mathbb{R})$. Note that the model simply describes a linear diffusion in the special case where $D(\rho) = -\tau\rho$ and $\tau < 0$.

3. Linear stability analysis.

3.1. Linear stability analysis of the continuous macroscopic model. In (15), the left-hand side is the LWR model with additional diffusion proportional to the reaction time parameter τ and that can be either negative or positive. More precisely, the diffusion is negative in deceleration phases where the density gets higher upstream, and it is positive in the opposite acceleration phases. This type of diffusion seems to induce an instability of the homogeneous (constant) solutions and the formation of oscillations (i.e., jam waves). The diffusion coefficient $(\rho V'(\rho))^2$ depends on the density and the fundamental diagram. In fluid dynamics the coefficient is a characteristic for the flexibility of the random movement responsible for the diffusion. In traffic flows, comparable diffusion-convection forms have been used in [31, 9]. We refer the interested reader to [9] (and references therein) for a proof of existence and uniqueness of the solution to (15)–(16). In the following we analyze the linear stability of homogeneous solutions for the macroscopic model at equilibrium density ρ_e.

PROPOSITION 1. *The homogeneous configurations for which $\rho(x,t) = \rho_e$ for all x and t are linearly stable for the continuous traffic model* (15) *if and only if*

$$\tau < 0. \tag{18}$$

Note that a negative τ refers to an anticipation time.

Proof. If $\varepsilon(x,t) = \rho(x,t) - \rho_e$ is a perturbation to homogeneous solution ρ_e, then

$$\varepsilon_t = F(\rho_e + \varepsilon, \varepsilon_x, \varepsilon_{xx}) = \alpha\varepsilon + \beta\varepsilon_x + \gamma\varepsilon_{xx} + o(LC(\varepsilon, \varepsilon_x, \varepsilon_{xx})), \tag{19}$$

with $F(\rho, \rho_x, \rho_{xx}) = -\partial_x\big(\rho V(\rho) - \tau(\rho V'(\rho))^2\partial_x\rho\big)$, $\alpha = \frac{\partial F}{\partial \rho}(\rho_e, \rho_e, \rho_e) = 0$, $\beta = \frac{\partial F}{\partial \rho_x} = -V(\rho_e) - \rho_e V'(\rho_e)$, $\gamma = \frac{\partial F}{\partial \rho_{xx}} = -\tau(\rho_e V'(\rho_e))^2$. The solutions of the linear system are the Ansatz $\varepsilon = ze^{\lambda t - ixl}$ where $\lambda \in \mathbb{C}$, $x, l \in \mathbb{R}$. We get $\varepsilon_t = \lambda\varepsilon$, $\varepsilon_x = -il\varepsilon$, and $\varepsilon_{xx} = -l^2\varepsilon$. Therefore, the characteristic equation of the perturbed system (19) is $\lambda_l = \tau(l\rho_e V'(\rho_e))^2 + il(V(\rho_e) + \rho_e V'(\rho_e))$. The homogeneous solutions are stable when $\varepsilon \to 0$, i.e., $\Re(\lambda_l) < 0$ for all $l > 0$. This holds only if the diffusion is positive. This is $\tau < 0$. ∎

Therefore, the macroscopic model is unstable as soon as the reaction time τ is positive, which is the physically reasonable case. An explanation is that the Taylor expansion of the original model in terms of τ does lead to a perturbed equation with different properties. However, the discrete model does not have this stability requirement. Therefore, we show below that for suitable discretization of the model we recover stability.

3.2. Linear stability analysis for the discrete schemes. Discretizations of the macroscopic models (12) and (13) in "Lagrangian" coordinates give the initial microscopic model (5). Our purpose in this section is the discretization of the macroscopic models (14) and (15) in Eulerian coordinates. We denote dt and dx the time and space discretization steps and use the Godunov scheme [21] for the discretization of the density

$$\rho_j(t + \mathsf{dt}) = \rho_j(t) + \frac{\mathsf{dt}}{\mathsf{dx}}\big(f_{j-1}(t) - f_j(t)\big), \tag{20}$$

where f_j denotes the flow at cell boundary and has to be determined. For this aim, we introduce the *demand* and *supply* functions from the flow-density fundamental diagram $Q : \rho \mapsto Q(\rho) := \rho V(\rho)$ as first proposed in [14, 27] and that read, respectively,

$$\Delta(\rho) := \max_{k \le \rho} Q(k) \quad \text{and} \quad \Sigma(\rho) := \max_{k \ge \rho} Q(k), \tag{21}$$

and we define the Godunov flux as $G(x,y) := \min\{\Delta(x), \Sigma(y)\}$. We are now ready to propose three different strategies to compute the boundary flows f_j. The first two methods discretize the linearized model (15) using a splitting scheme which treats the convection and the diffusion terms separately. The last scheme is a simple discretization of the exact macroscopic model (14).

1. *The Godunov/Euler scheme:* A Godunov scheme for the convection term and an explicit Euler scheme for the diffusive term of the linearized model (15):

$$f_j^{(1)} = G(\rho_j, \rho_{j+1}) + \frac{\tau}{\mathsf{dx}}(\rho_j V'(\rho_j))^2(\rho_{j+1} - \rho_j). \tag{22}$$

   Such a scheme is the one used in [2].
2. *The Godunov/Godunov scheme:* A Godunov scheme for the convection term and a Godunov scheme for the diffusion term of the Taylor-expanded model (15):

$$f_j^{(2)} = G(\rho_j, \rho_{j+1}) + \frac{\tau}{\mathsf{dx}}\rho_j V'(\rho_j)\big[G(\rho_{j+1}, \rho_{j+2}) - G(\rho_j, \rho_{j+1})\big]. \tag{23}$$

3. *The Godunov scheme:* A Godunov scheme for the modified convection term in the exact macroscopic model (14):

$$f_j^{(3)} = G\left(\frac{\rho_j}{1 - \frac{\tau}{\mathsf{dx}}\big(V(\rho_{j+1}) - V(\rho_j)\big)}, \frac{\rho_{j+1}}{1 - \frac{\tau}{\mathsf{dx}}\big(V(\rho_{j+2}) - V(\rho_{j+1})\big)}\right). \tag{24}$$

   Note that this scheme is valid if $1 - \frac{\tau}{\mathsf{dx}}\big(V(\rho_{j+1}) - V(\rho_j)\big) > 0$ for all ρ_j and ρ_{j+1}. By denoting $V_0 = \sup_x V(x)$, this inequality holds if

$$\tau < \mathsf{dx}/V_0. \tag{25}$$

PROPOSITION 2. *In a system of K cells with periodic boundary conditions, the homogeneous configurations for which $\rho_j(t) = \rho_e$ for all j and t are linearly stable for the discrete traffic model* (20) *if and only if*

$$\alpha^2 + \beta^2 + \gamma^2 + \xi^2 - 2\alpha\gamma - 2\beta\xi + 2h(c_l) < 1 \qquad \forall l = 1, \ldots, K-1, \tag{26}$$

with $c_l = \cos(2\pi l/K)$ and $h(x) = (\alpha\beta + \alpha\xi + \beta\xi - 3\gamma\xi)x + 2(\alpha\gamma + \beta\xi)x^2 + 4\gamma\xi x^3$, and $\alpha = \frac{\partial F}{\partial \rho_j}$, $\beta = \frac{\partial F}{\partial \rho_{j+1}}$, $\gamma = \frac{\partial F}{\partial \rho_{j+2}}$, and $\xi = \frac{\partial F}{\partial \rho_{j-1}}$ the partial derivatives of the model in equilibrium.

Proof. The perturbations to homogeneous solution are the variables $\varepsilon_j(t) = \rho_j(t) - \rho_e$. The perturbed system is

$$\begin{aligned} \varepsilon_j(t + \mathsf{dt}) &= \rho_j(t + \mathsf{dt}) - \rho_e = F(\rho_j(t), \rho_{j+1}(t), \rho_{j+2}(t), \rho_{j-1}(t)) - \rho_e \\ &= \alpha\,\varepsilon_j(t) + \beta\,\varepsilon_{j+1}(t) + \gamma\,\varepsilon_{j+2}(t) + \xi\,\varepsilon_{j-1}(t) + o(\mathrm{LC}(\varepsilon_j, \varepsilon_{j-1}, \varepsilon_{j+1}, \varepsilon_{j+2})), \end{aligned} \tag{27}$$

with $\alpha = \frac{\partial F}{\partial \rho_j}$, $\beta = \frac{\partial F}{\partial \rho_{j+1}}$, $\gamma = \frac{\partial F}{\partial \rho_{j+2}}$, and $\xi = \frac{\partial F}{\partial \rho_{j-1}}$ at $(\rho_e, \rho_e, \rho_e, \rho_e)$. General conditions for the global stability of the discrete schemes can be obtained for a system of K cells with periodic boundary conditions for which the equilibrium density $\rho_e = N/(K\,\mathsf{dx})$, N being the number of agents. The linear perturbed system is $\vec{\varepsilon}(t + \mathsf{dt}) = M\,\vec{\varepsilon}(t)$, with $\vec{\varepsilon} = {}^{\mathrm{T}}(\varepsilon_1, \ldots, \varepsilon_K)$ and M a sparse matrix with $(\xi, \alpha, \beta, \gamma)$ on the diagonal. If $M = PDP^{-1}$ with D a diagonal matrix, then $\vec{\varepsilon}(t) = PD^{t/\mathsf{dt}}P^{-1}\,\vec{\varepsilon}(0) \to \vec{0}$

if all the coefficients of D are less than 1, except for one coefficient which is equal to 1. M is circulant; therefore, the eigenvectors of M are $z(\iota^0, \iota^1, \dots, \iota^{m-1})$ with $\iota = \exp\left(i\frac{2\pi l}{K}\right)$ and $z \in \mathbb{Z}$, and the eigenvalues are $\lambda_l = \alpha + \beta\iota_l + \gamma\iota_l^2 + \xi\iota_l^{-1}$. The system is linearly stable if $|\lambda_l| < 1$ for all $l = 1, \dots, K-1$. This is

$$\lambda_l^2 = \alpha^2 + \beta^2 + \gamma^2 + \xi^2 - 2\alpha\gamma - 2\beta\xi + 2h(c_l) < 1 \qquad \forall l = 1, \dots, K-1, \tag{28}$$

with $c_l = \cos(2\pi l/K)$ and $h(x) = (\alpha\beta + \alpha\xi + \beta\xi - 3\gamma\xi)x + 2(\alpha\gamma + \beta\xi)x^2 + 4\gamma\xi x^3$. ∎

These conditions (26) are applied to the different numerical schemes (22), (23), and (24) with optimal speed $V(\rho) = \frac{1}{T}(1/\rho - \ell)$, $T > 0$ being the vehicles' time gap and $\ell \geq 0$ the vehicles' size. For such speed functions, the Godunov scheme is simply $G(x, y) = \frac{1}{T}(1 - y\ell)$.

LEMMA 3. *The homogeneous configurations are linearly stable for the Godunov/Euler scheme* (20)–(22) *if*

$$2\tau < T\ell\,\mathsf{dx}\,\rho_e^2, \tag{29}$$

and if dt *is sufficiently small.*

Proof. Mixed with the scheme for the density (20), Godunov/Euler scheme (22) is

$$F_1(\rho_j, \rho_{j+1}, \rho_{j+2}, \rho_{j-1}) = \rho_j + \frac{\mathsf{dt}}{T\,\mathsf{dx}}\left(\ell(\rho_{j+1} - \rho_j) + \frac{\tau}{T\,\mathsf{dx}}\left(\frac{\rho_j - \rho_{j-1}}{\rho_{j-1}^2} - \frac{\rho_{j+1} - \rho_j}{\rho_j^2}\right)\right), \tag{30}$$

where $\alpha = 1 - A + 2B$, $\beta = A - B$, $\gamma = 0$, and $\xi = -B$ with $A = \frac{\mathsf{dt}\,\ell}{T\,\mathsf{dx}}$ and $B = \frac{\mathsf{dt}\,\tau}{(T\,\mathsf{dx}\,\rho_e)^2}$.

If $\tau < \frac{1}{2}T\ell\,\mathsf{dx}\,\rho_e^2$, then $\alpha > 0$ for

$$\mathsf{dt} < \frac{T\,\mathsf{dx}}{\ell + \frac{2\tau}{T\,\mathsf{dx}\,\rho_e^2}}, \tag{31}$$

and for all $\mathsf{dt} \geq 0$ if $\tau \geq \frac{1}{2}T\ell\,\mathsf{dx}\,\rho_e^2$. Moreover, $1 - \alpha > 0$ if $\tau < \frac{1}{2}T\ell\,\mathsf{dx}\,\rho_e^2$, while β is positive only if $\tau < T\ell\,\mathsf{dx}\,\rho_e^2$ and the sign of ξ is the one of $-\tau$.

The stability conditions are distinguished according to the sign of τ.

- If $\tau < 0$ and (31) holds, then $h(x) = \alpha(1-\alpha)x + 2\beta\xi x^2$ is strictly convex and is maximal on $[-1, 1]$ for $x = -1$ or $x = 1$. Therefore, the model is stable if $h(-1) < h(1)$; this is simply $-\alpha(1-\alpha) < \alpha(1-\alpha)$, which is always true since $\alpha > 0$ if (31) holds and $1 - \alpha > 0$ on $\tau < 0$. Therefore, the system is stable for all $\tau < 0$.
- Several cases have to be distinguished for $\tau > 0$. We assume in the following that (31) holds.
  - For $0 < \tau < \frac{1}{2}T\ell\,\mathsf{dx}\,\rho_e^2$, we have $\alpha, 1 - \alpha, \beta > 0$, $\xi < 0$, and $h(x) = \alpha(1-\alpha)x + 2\beta\xi x^2$ is strictly concave and maximal for $x_0 = -\frac{\alpha(1-\alpha)}{4\beta\xi} > 0$. The model is stable if $x_0 > 1$; this is

    $$\mathsf{dt} < \frac{T\,\mathsf{dx}}{\ell} - \frac{2\tau}{(\ell\rho_e)^2}. \tag{32}$$

    This condition is more restrictive than (31).

– For $\frac{1}{2}T\ell\,\mathsf{dx}\,\rho_e^2 < \tau < T\ell\,\mathsf{dx}\,\rho_e^2$, we have $\alpha, \beta > 0$, $1-\alpha, \xi < 0$, and $h(-1) > h(1)$; therefore, the model is unstable. More precisely, h maximal for $x_0 < -1$; i.e., the unstable solutions have the shortest wavelength if

$$\mathsf{dt} < \left(\tau - \frac{1}{2}T\ell\,\mathsf{dx}\,\rho_e^2\right)\left(\frac{2\tau}{T\,\mathsf{dx}\,\rho_e}\right)^{-2}. \tag{33}$$

This condition is also more restrictive than (31).

– For $\tau > T\ell\,\mathsf{dx}\,\rho_e^2$, we have $\alpha > 0$, $1-\alpha, \beta, \xi < 0$, and the system is unstable for all dt with shortest wavelength since $h(\cdot)$ is strictly convex and $h(-1) > h(1)$. ∎

The stability conditions for the Godunov/Euler splitting scheme (22) are summarized in Figure 2. The same conditions as the continuous macroscopic model are obtained for $\mathsf{dx} \to 0$ and $\mathsf{dt} \to 0$ such that $\mathsf{dt}\,/\,\mathsf{dx} \to 0$. At the limit $\mathsf{dt} \to 0$, the stability does not occur as soon as the reaction time τ is positive if the space discretization dx is sufficiently small. Large dx may lead to stability even if τ is positive due to numerical stabilization.

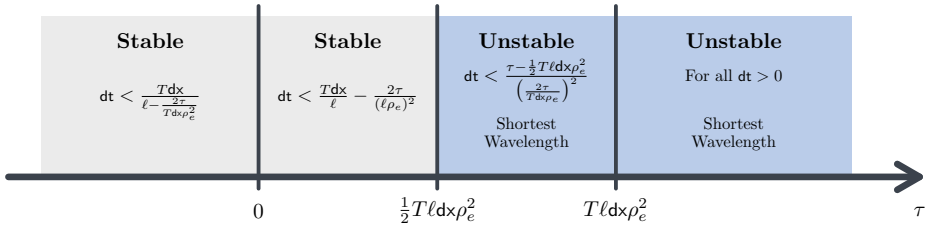

FIG. 2. *Summary of the stability conditions for the Godunov/Euler splitting scheme* (22).

LEMMA 4. *The homogeneous configurations are linearly stable for the Godunov/Euler schemes* (20)–(23) *and* (20)–(24) *if*

$$2|\tau| < T\,\mathsf{dx}\,\rho_e, \tag{34}$$

and if dt *is sufficiently small.*

Proof. The Godunov numerical schemes (23) and (24) are, respectively,

$$F_2(\rho_j, \rho_{j+1}, \rho_{j+2}, \rho_{j-1}) = \rho_j + \frac{\mathsf{dt}\,\ell}{T\,\mathsf{dx}}\left(\rho_{j+1} - \rho_j + \frac{\tau}{T\,\mathsf{dx}}\left(\frac{\rho_{j+1} - \rho_{j+2}}{\rho_j} - \frac{\rho_j - \rho_{j+1}}{\rho_{j-1}}\right)\right) \tag{35}$$

and

$$F_3(\rho_j, \rho_{j+1}, \rho_{j+2}, \rho_{j-1}) = \rho_j + \frac{\mathsf{dt}\,\ell}{T\,\mathsf{dx}}\left(\frac{\rho_{j+1}}{1 - \frac{\tau}{T\,\mathsf{dx}}\left(\frac{1}{\rho_{j+2}} - \frac{1}{\rho_{j+1}}\right)} - \frac{\rho_j}{1 - \frac{\tau}{T\,\mathsf{dx}}\left(\frac{1}{\rho_{j+1}} - \frac{1}{\rho_j}\right)}\right). \tag{36}$$

By construction, both give $\alpha = 1 - A(1+B)$, $\beta = A(1+2B)$, $\gamma = -AB$, and $\xi = 0$ with $A = \frac{\mathsf{dt}\,\ell}{T\,\mathsf{dx}}$ and $B = \frac{\tau}{T\,\mathsf{dx}\,\rho_e}$. As expected, the stability conditions of these two schemes are the same.

If $\tau > -T\,\mathsf{dx}\,\rho_e$, then $\alpha > 0$ for

$$\mathsf{dt} < \frac{T\,\mathsf{dx}}{\ell + \frac{\ell\tau}{T\,\mathsf{dx}\,\rho_e}}, \tag{37}$$

and for all $\mathsf{dt} \geq 0$ if $\tau \leq -T\,\mathsf{dx}\,\rho_e$. β is positive only if $\tau > -\frac{1}{2}T\,\mathsf{dx}\,\rho_e$. Moreover, $1-\beta > 0$ if (37) holds, while the sign of γ is the one of $-\tau$.

Here again, the stability conditions are distinguished according to the sign of τ.

- If $\tau < 0$ and (37) holds, $h(x) = \beta(1-\beta)x + 2\alpha\gamma x^2$ is strictly convex and maximal on $[-1,1]$ for $x = -1$ or $x = 1$. Therefore, the model is stable if $h(-1) < h(1)$; this is

$$\tau > -\frac{1}{2}T\,\mathsf{dx}\,\rho_e \qquad \text{and} \qquad \mathsf{dt} < \frac{T\,\mathsf{dx}}{\ell + \frac{2\ell\tau}{T\,\mathsf{dx}\,\rho_e}}. \tag{38}$$

  The condition for dt is weaker than (37) since τ is negative. If $\tau \leq -\frac{1}{2}T\,\mathsf{dx}\,\rho_e$, then the system is unstable at the shortest wavelength frequency. A sufficient condition for the finite system producing the shortest frequency is simply $K \geq 2$. Note that no condition holds on dt if $\tau \leq -T\,\mathsf{dx}\,\rho_e$.
- If $\tau > 0$ and (37) holds, then $h(x) = \beta(1-\beta)x + 2\alpha\gamma x^2$ is concave and is maximum at $\arg\sup_x h(x) = x_0 = -\frac{\beta(1-\beta)}{4\alpha\gamma} > 0$. We know that $\lambda_0^2 = \alpha^2 + \beta^2 + \gamma^2 - 2\alpha\beta + h(1) = 1$ (case $l = 0$). Therefore, the model is stable if $x_0 > 1$; this is

$$\tau < \frac{1}{2}T\,\mathsf{dx}\,\rho_e \qquad \text{and} \qquad \mathsf{dt} < \frac{T\,\mathsf{dx}}{\ell} - \frac{2\tau}{\ell\rho_e}. \tag{39}$$

  The condition for dt is stronger than (37). If $\tau \geq \frac{1}{2}T\,\mathsf{dx}\,\rho_e$, then the system is unstable at the frequency $\cos^{-1}(x_0)$ that is reachable in the finite system if $K > 2\pi/\cos^{-1}(x_0)$. We have $x_0 \to 1/2 + T\,\mathsf{dx}\,\rho_e/(4\tau)$ as $\mathsf{dt} \to 0$, going from 1 to $1/2$ according to τ (long wave). ∎

The stability conditions for the Godunov/Godunov and Godunov schemes (23) and (24) are summarized in Figure 3. The same conditions as the microscopic model are obtained at the limit $\mathsf{dt} \to 0$ for $\mathsf{dx} = 1/\rho_e$, i.e., a space step equal to the mean spacing. In this case, the stability occurs when the absolute value of the reaction time τ is smaller than two times the time gap T (see (6) and [4]).

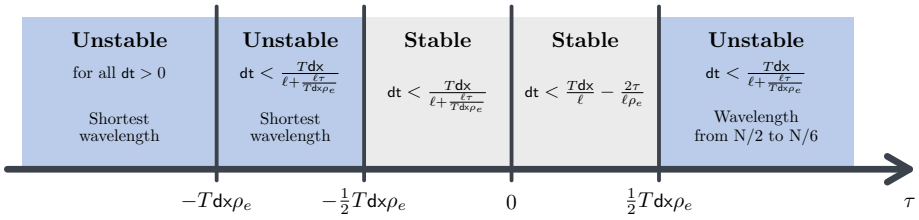

FIG. 3. *Summary of the stability conditions for the Godunov/Godunov and Godunov schemes* (23) *and* (24). *Note that we have the additional condition* $\tau < \mathsf{dx}/V_0$, *with* $V_0 = \sup_x V(x)$, *for the simple Godunov scheme* (24).

3.3. Bounds on the speed and the density. The microscopic model (5) is collision-free: the spacing remains by construction bigger than the vehicle length $\ell > 0$, and the speed is positive and bounded. We check whether this property also occurs with the numerical schemes F_n, $n = 1, 2, 3$, of the macroscopic models (30), (35), and (36). The models are of the first order; therefore, the speed is necessarily positive and bounded if the optimal velocity functions are so defined. Moreover, the

density remains bounded in $[1, \rho_M]$, with $\rho_M = 1/\ell$, if

$$F_n(0, a, b, c) \geq 0 \quad \text{and} \quad F_n(\rho_M, a, b, c) \leq \rho_M \qquad \forall\, (a, b, c). \tag{40}$$

It is easy to check that such a property holds only if $\tau \leq 0$ for the Godunov/Euler equation (30), while it holds for $\tau \geq -\,\mathsf{dx}\,\rho_e/W'$ with the Godunov/Godunov scheme (35), and for $\tau < \mathsf{dx}/V_0$ with the simple Godunov scheme (36). The nonlinear part of the diffusion term $-\tau\partial_x\left((\rho V'(\rho))^2\partial_x\rho\right)$ in (15) allows us to avoid unrealistic unbounded density level phenomena that can be obtained by using linear diffusion models (see [14, 3]).

As the microscopic model, (35) and (36) are able to describe macroscopically unstable homogeneous solutions with large waves by ensuring that speed and density remain positive and bounded. The relation between instability and self-sustained traffic waves (or jamitons) are notably described in [18, 35, 36, 42] with microscopic and macroscopic second order models. In the next section, we analyze by simulation the unstable solutions we get with the first order models for different initial conditions.

4. Simulation results. In this section numerical simulations of the microscopic model (5) and of the simple Godunov scheme (36) macroscopic model are compared. The car-following model (5) is simulated using an explicit Euler scheme. A ring (periodic boundaries) with a length 101 and 50 vehicles is considered. The optimal speed functions are $W(\Delta) = \max\{0, \min\{2, \Delta - 1\}\}$ and $V(\rho) = W(1/\rho)$ corresponding to a triangular fundamental diagram, while the reaction time is $\tau = 1$. The values of the parameters are set to obtain unstable homogeneous solutions. The time step is $\mathsf{dt} = 0.01$. The space step for the Godunov scheme is the mean spacing $\mathsf{dx} = 101/50 = 2.02$ in order to match the stability conditions of both microscopic and macroscopic models (see (6) and Figure 3) and to hold the CFL conditions (see (25) and Figure 3). Three experiments are carried out with different initial conditions. In the first one, the initial configuration is a jam. The initial condition is random in the second experiment, while it is a perturbed homogeneous configuration in the last one.

4.1. Trajectories. In Figures 4, 5, and 6, the trajectories of the microscopic model and the time series for the density by cell for the discrete macroscopic model (gray levels) are plotted for, respectively, the jam, random, and perturbed initial conditions. The jam propagation is stationary within the first experiment in Figure 4. Both microscopic and macroscopic models rigorously describe the same dynamics. The dynamics obtained does not perfectly coincide for the random and perturbed initial conditions (see Figures 5 and 4). Yet most of the dynamics seems to be well recaptured—notably the self-sustained emergence of traffic stop-and-go waves. Note that the waves propagate backward with the speed $-\ell/T$ that is close to the value empirically observed (see [33]).

4.2. Fundamental diagram. The fundamental diagram is the plot of the flow or the mean speed as a function of the density. It generally refers to spatial performances [16] that have to be distinguished from temporal ones [46]. Here, to deal with spatial performances, we measured the spatial speed and the density and expressed the flow as the product of the density by the speed. The density for the microscopic model is the inverse of the spacing (see (7)), while the speed in the macroscopic model is (see (9))

$$\tilde{V}(\rho_j, \rho_{j+1}) = V\left(\frac{\rho}{1 - \tau\rho(V(\rho_{j+1}) - V(\rho_j))}\right). \tag{41}$$

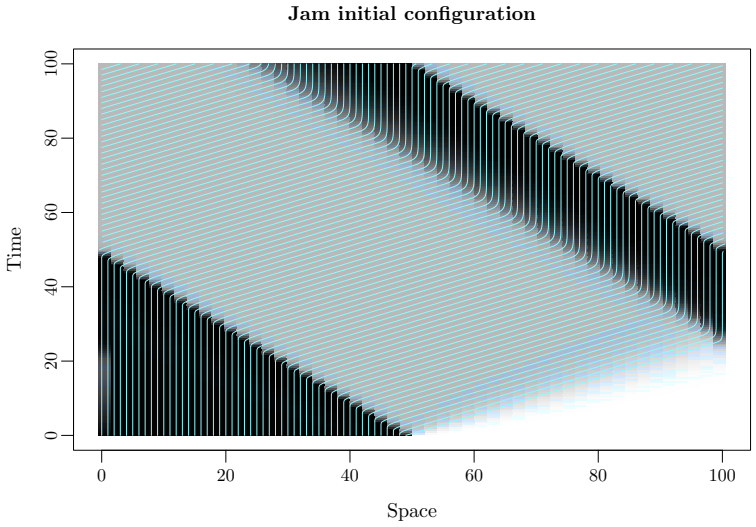

FIG. 4. *The trajectories of the microscopic model (cyan curves) and the time series for the density by cell for the discrete macroscopic model (gray levels) for jam initial conditions.*

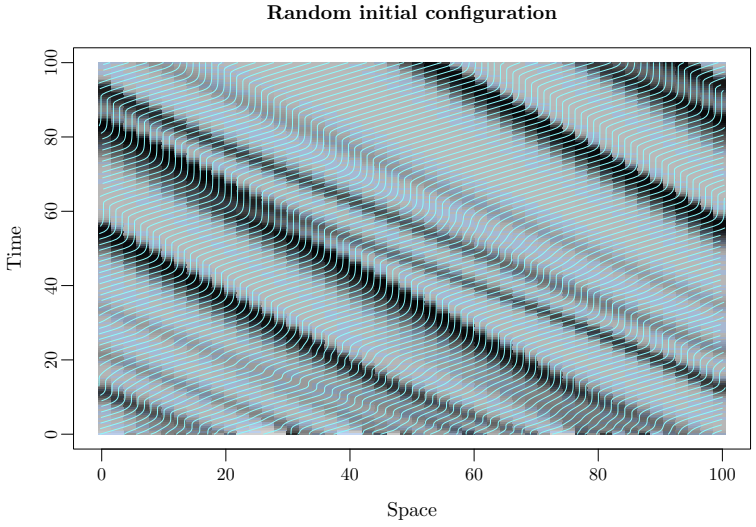

FIG. 5. *The trajectories of the microscopic model (cyan curves) and the time series for the density by cell for the discrete macroscopic model (gray levels) for random initial conditions.*

The sequences obtained for the perturbed initial conditions (see Figure 6) are presented in Figure 7. The performances are *instantaneous* ones in the sense that they correspond to instantaneous measurements for a vehicle (microscopic model) and a cell (macroscopic model) in the system. The variability in such a diagram is larger than that of the *aggregated* fundamental diagram plotted in [24, Figure 1] and [49, Figure 5], where the performances were averaged over time intervals.

Both microscopic and macroscopic systems converge to limit-cycles with self-

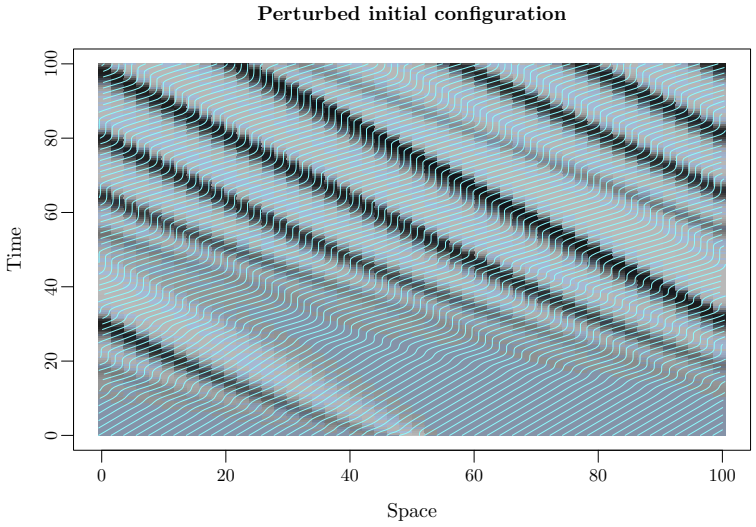

FIG. 6. *The trajectories of the microscopic model (cyan curves) and the time series for the density by cell for the discrete macroscopic model (gray levels) for perturbed initial conditions.*

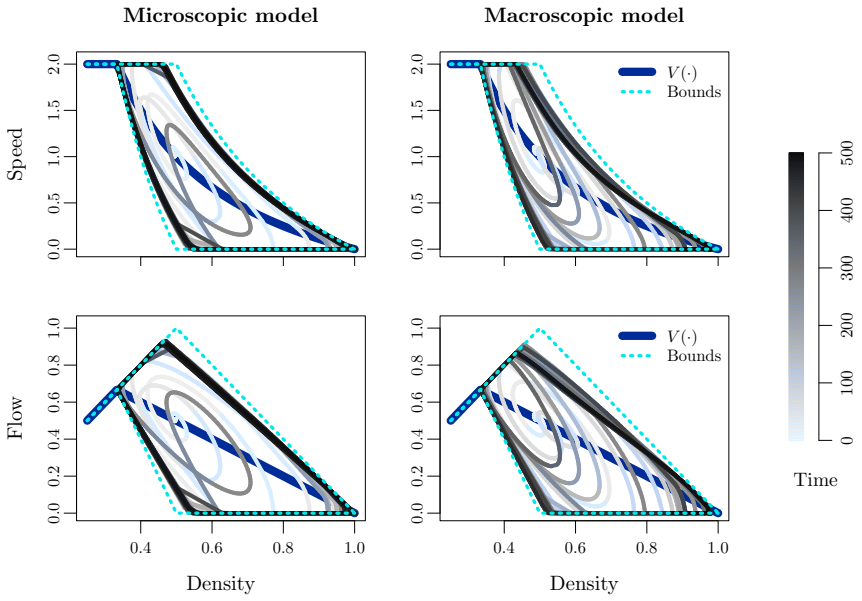

FIG. 7. *Sequence of speed and flow/density relation for the perturbed initial conditions (see Figure 6). Left, for one vehicle (microscopic model), and right, for one cell (macroscopic model).*

sustained stop-and-go waves resulting in hysteresis curves in the microscopic fundamental diagram. Such phenomena generate scattering of the fundamental diagram for which some bounds can be calculated [48, 12, 20, 13, 42, 17]. The bounds V^+ and V^- for the fundamental diagrams can here intuitively be determined from the microscopic model. The upper bound V^+ corresponds to the sequence of a vehicle

moving at maximal speed V_0 behind a stopped vehicle:

$$V^+(\rho) = \tilde{V}(\rho, 1/\ell) = V\left(\frac{\rho}{1+\tau\rho V(\rho)}\right). \tag{42}$$

Due to the reaction time, the distance tends to be smaller and the fundamental diagram is "overestimated." Oppositely, the lower bound V^- corresponds to the sequence of a stopped vehicle following a predecessor moving at the maximal speed V_0:

$$V^-(\rho) = \tilde{V}(\rho_j, 0) = V\left(\frac{\rho}{1-\tau\rho(V_0 - V(\rho))}\right). \tag{43}$$

Here the reaction time induces a delay in the acceleration and an underestimation of the fundamental diagram.

As in [42, 17], the bounds (42) and (43) obtained with the macroscopic model are compared to real instantaneous pedestrian and road traffic data in Figures 8 and 9. The pedestrian data comes from a laboratory experiment with participants in a ring geometry [19]. Several experiments have been carried out with different density levels. The road traffic data are real measurements of trajectories on an American highway [34]. The speed, density, and flow are measured as previously (i.e., the density is the inverse of the spacing, while the flow is the product of the density by the speed). A triangular fundamental diagram with three parameters $V(\rho) = \min\left\{V_0, \frac{1}{T}(1/\rho - 1)\right\}$ is used again. The parameters are those of an estimation by least squares for the pedestrians $V_0 = 0.9$ m/s, $\ell = 0.3$ m, and $T = \tau = 1$ s (see Figure 8), while $V_0 = 15$ m/s, $\ell = 5$ m, and $T = \tau = 2$ s for the vehicles (see Figure 9). The bounds present a reasonable agreement with the data, even if no clustering of measurements is observed around them.

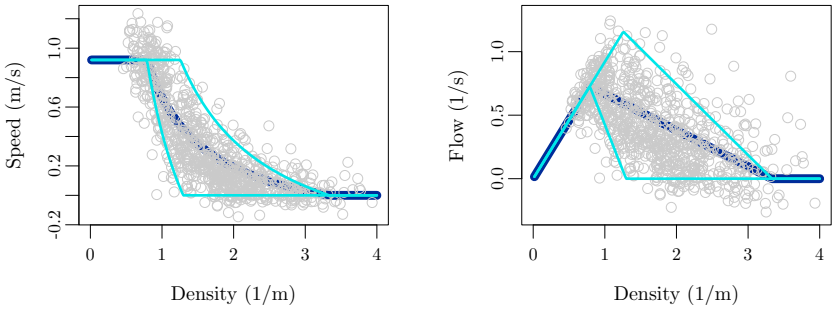

FIG. 8. *Instantaneous speed/density and flow/density measurements for real pedestrian flows* [19] *and the bounds* (42) *and* (43) *for* $V_0 = 0.9$ *m/s,* $\ell = 0.3$ *m, and* $T = \tau = 1$ *s.*

5. Conclusion. Starting from a speed-following model, we derive a parabolic convection-diffusion continuum traffic flow model that we discretized using Godunov and Euler schemes. Simulation results show that discrete macroscopic models can recapture the dynamics of the microscopic model if specific values for the space discretization are chosen. More precisely, the linear stability conditions of the homogeneous solutions for the macroscopic models match those of the microscopic model for specific values of the space discretization and sufficiently small time steps.

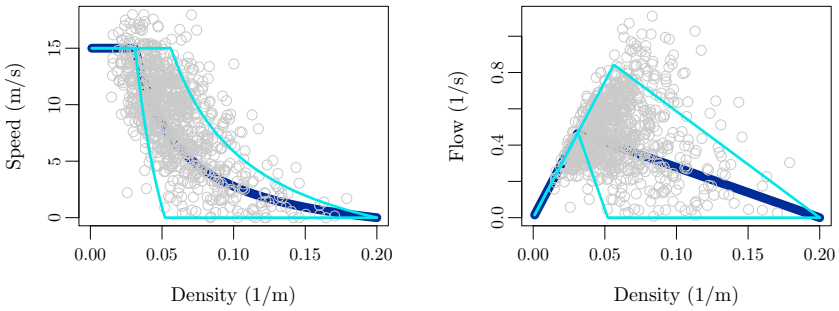

FIG. 9. *Individual speed/density and flow/density measurements for real road traffic flows* [34] *and the bounds* (42) *and* (43) *for* $V_0 = 15$ *m/s,* $\ell = 5$ *m, and* $T = \tau = 2$ *s.*

For unstable conditions, i.e., for large reaction times, the dynamics obtained describe self-sustained stop-and-go waves, with hysteresis cycles and a large scattering of the fundamental flow/density diagram. Such characteristics are observed in real data [45, 25, 24, 10, 49] as well as for second order models [48, 12, 20, 6, 18, 42, 13, 17]. Here it is achieved with first order models ensuring by construction that the models are physical and "collision-free" (i.e., bounded and having positive speed as well as density). Further investigations are necessary to understand the impact of the shape of the optimal velocity function on the characteristics of the waves.

The macroscopic model corresponding to the follow-the-leader model is a first order elliptic convection-diffusion equation, for which the convection part is calibrated by the optimal velocity function (i.e., the fundamental diagram), while the diffusion is proportional to the reaction time parameter. More precisely, the diffusion is negative in deceleration phases where the density increases, and it is positive in acceleration phases where the density decreases. Such a mechanism seems to be responsible for the appearance of oscillations and self-sustained nonlinear stop-and-go waves in the system. This observation remains to be confirmed rigorously, yet it could give us a way to explain the wave formations.

REFERENCES

[1] C. Appert-Rolland, P. Degond, and S. Motsch, *Two-way multi-lane traffic model for pedestrians in corridors*, Netw. Heterog. Media, 6 (2011), pp. 351–381.

[2] A. Aw, A. Klar, T. Materne, and M. Rascle, *Derivation of continuum traffic flow models from microscopic follow-the-leader models*, SIAM J. Appl. Math., 63 (2002), pp. 259–278, https://doi.org/10.1137/S0036139900380955.

[3] A. Aw and M. Rascle, *Resurrection of "second order" models of traffic flow*, SIAM J. Appl. Math., 60 (2000), pp. 916–938, https://doi.org/10.1137/S0036139997332099.

[4] M. Bando, K. Hasebe, A. Nakayama, A. Shibata, and Y. Sugiyama, *Dynamical model of traffic congestion and numerical simulation*, Phys. Rev. E, 51 (1995), pp. 1035–1042.

[5] A. M. Bayen and C. G. Claudel, *Lax-Hopf based incorporation of internal boundary conditions into Hamilton-Jacobi equation. Part* I: *Theory*, IEEE Trans. Automat. Control, 55 (2010), pp. 1142–1157.

[6] F. Berthelin, P. Degond, M. Delitala, and M. Rascle, *A model for the formation and evolution of traffic jams*, Arch. Ration. Mech. Anal., 187 (2008), pp. 185–220.

[7] S. Blandin, D. Work, P. Goatin, B. Piccoli, and A. Bayen, *A general phase transition model for vehicular traffic*, SIAM J. Appl. Math., 71 (2011), pp. 107–127, https://doi.org/10.1137/090754467.

[8] I. Bonzani, *Hydrodynamic models of traffic flow: Drivers' behaviour and nonlinear diffusion*, Math. Comput. Model., 31 (2000), pp. 1–8.
[9] R. Bürger and K. H. Karlsen, *On a diffusively corrected kinematic-wave traffic flow model with changing road surface conditions*, Math. Models Methods Appl. Sci., 13 (2003), pp. 1767–1799.
[10] D. Chowdhury, L. Santen, and A. Schadschneider, *Statistical physics of vehicular traffic and some related systems*, Phys. Rep., 329 (2000), pp. 199–329.
[11] M. Chraibi, U. Kemloh, A. Schadschneider, and A. Seyfried, *Force-based models of pedestrian dynamics*, Netw. Heterog. Media, 6 (2011), pp. 425–442.
[12] R. Colombo, *Hyperbolic phase transitions in traffic flow*, SIAM J. Appl. Math., 63 (2002), pp. 708–721, https://doi.org/10.1137/S0036139901393184.
[13] R. Colombo, F. Marcellini, and M. Rascle, *A 2-phase traffic model based on a speed bound*, SIAM J. Appl. Math., 70 (2010), pp. 2652–2666, https://doi.org/10.1137/090752468.
[14] C. F. Daganzo, *Requiem for second-order fluid approximations of traffic flow*, Transport. Res. B Meth., 29 (1995), pp. 277–286.
[15] L. C. Davis, *Modifications of the optimal velocity traffic model to include delay due to driver reaction time*, Phys. A, 319 (2003), pp. 557–567.
[16] L. Edie, *Discussion of traffic stream measurements and definitions*, in Proceedings of the 2nd International Symposium on Transportation and Traffic Theory, J. Almond, ed., Paris, France, 1963, pp. 139–154.
[17] S. Fan, M. Herty, and B. Seibold, *Comparative model accuracy of a data-fitted generalized Aw-Rascle-Zhang model*, Netw. Heterog. Media, 9 (2014), pp. 239–268.
[18] M. Flynn, A. Kasimov, J.-C. Nave, R. Rosales, and B. Seibold, *Self-sustained nonlinear waves in traffic flow*, Phys. Rev. E, 79 (2009), 056113.
[19] Forschungszentrum Jülich, *Division Civil Safety and Traffic*, http://ped.fz-juelich.de/database.
[20] P. Goatin, *The Aw–Rascle vehicular traffic flow model with phase transitions*, Math. Comput. Model., 44 (2006), pp. 287–303.
[21] S. K. Godunov, *A difference scheme for the numerical computation of a discontinuous solution of the hydrodynamic equation*, Math. Sbornik, 47 (1959), pp. 271–306.
[22] J. Greenberg, *Extensions and amplifications of a traffic model of Aw and Rascle*, SIAM J. Appl. Math., 62 (2001), pp. 729–745, https://doi.org/10.1137/S0036139900378657.
[23] D. Helbing, *Verkehrsdynamik. Neue physikalische Modellierungskonzepte*, Springer-Verlag, Berlin, 1997.
[24] B. S. Kerner, *Phase transitions in traffic flow*, in Traffic and Granular Flow '99, D. Helbing, H. J. Herrmann, M. Schreckenberg, and D. E. Wolf, eds., Springer-Verlag, Berlin, Heidelberg, 2000, pp. 253–283.
[25] B. S. Kerner and H. Rehborn, *Experimental properties of phase transitions in traffic flow*, Phys. Rev. Lett., 79 (1997), pp. 4030–4033.
[26] J.-P. Lebacque, *Les modeles macroscopiques du traffic*, Annales des Ponts, 67 (1993), pp. 24–45.
[27] J.-P. Lebacque, *The Godunov scheme and what it means for first order traffic flow models*, in Proceedings of the 13th International Symposium on Transportation and Traffic Theory, J.-B. Lesort, ed., Lyon, France, 1996, pp. 647–677.
[28] J.-P. Lebacque, H. Haj-Salem, and S. Mammar, *Second order traffic flow modeling: Supply-demand analysis of the inhomogeneous Riemann problem and of boundary conditions*, in Proceedings of the 10th Euro Working Group on Transportation (EWGT), Poznan, Poland, 2005, pp. 108–115.
[29] J.-P. Lebacque, S. Mammar, and H. H. Salem, *Generic second order traffic flow modelling*, in Proceedings of the 17th Symposium on Transportation and Traffic Theory, Elsevier, Oxford, UK, 2007, pp. 755–776.
[30] M. H. Lighthill and G. B. Whitham, *On kinematic waves* II: *A theory of traffic flow on long, crowded roads*, Proc. Roy. Soc. London Ser. A, 229 (1955), pp. 317–345.
[31] P. Nelson, *Synchronized traffic flow from a modified Lighthill–Whitman model*, Phys. Rev. E, 61 (2000), pp. R6052–R6055.
[32] G. F. Newell, *Nonlinear effects in the dynamics of car-following*, Oper. Res., 9 (1961), pp. 209–229.
[33] K. Nishinari, M. Treiber, and D. Helbing, *Interpreting the wide scattering of synchronized traffic data by time gap statistics*, Phys. Rev. E, 68 (2003), 067101.
[34] U. D. of Transportation, *NGSIM: Next Generation Simulation*, http://www.ngsim.fhwa.dot.gov.

[35] G. Orosz and G. Stépán, *Subcritical Hopf bifurcations in a car-following model with reaction-time delay*, Proc. Roy. Soc. Lond. Ser. A Math. Phys. Eng. Sci., 462 (2006), pp. 2643–2670.
[36] G. Orosz, R. E. Wilson, and G. Stépán, *Traffic jams: Dynamics and control*, Philos. Trans. R. Soc. Lond. Ser. A Math. Phys. Eng. Sci., 368 (2010), pp. 4455–4479.
[37] G. Orosz, R. E. Wilson, R. Szalai, and G. Stépán, *Exciting traffic jams: Nonlinear phenomena behind traffic jam formation on highways*, Phys. Rev. E, 80 (2009), 046205.
[38] H. J. Payne, *Models of freeway traffic and control*, in Mathematical Models of Public Systems, Simulation Council Proceedings Series 1, Simulation Council, La Jolla, CA, 1971, pp. 51–61.
[39] L. A. Pipes, *An operational analysis of traffic dynamics*, J. Appl. Phys., 24 (1953), pp. 274–281.
[40] P. I. Richards, *Shock waves on a highway*, Oper. Res., 4 (1956), pp. 42–51.
[41] A. Schadschneider and A. Seyfried, *Empirical results for pedestrian dynamics and their implications for modeling*, Netw. Heterog. Media, 6 (2011), pp. 545–560.
[42] B. Seibold, M. Flynn, A. Kasimov, and R. Rosales, *Constructing set-valued fundamental diagrams from jamiton solutions in second order traffic models*, Netw. Heterog. Media, 8 (2013), pp. 745–772.
[43] A. Tordeux and A. Seyfried, *Collision-free nonuniform dynamics within continuous optimal velocity models*, Phys. Rev. E, 90 (2014), 042812.
[44] M. Treiber and A. Kesting, *Traffic Flow Dynamics*, Springer, Berlin, 2013.
[45] J. Treiterer and J. Myers, *The hysteresis phenomenon in traffic flow*, in Proceedings of the 6th International Symposium on Transportation and Traffic Theory, D. J. Buckley, ed., Sydney, Australia, 1974, pp. 13–38.
[46] J. Wardrop, *Some theoretical aspects of road traffic research*, Proc. ICE, 1 (1952), pp. 325–362.
[47] G. Whitham, *Linear and Nonlinear Waves*, Pure Appl. Math., Wiley, New York, 1974.
[48] H. Zhang, *A non-equilibrium traffic model devoid of gas-like behavior*, Transport. Res. B Meth., 36 (2002), pp. 275–290.
[49] J. Zhang, W. Mehner, S. Holl, M. Boltes, E. Andresen, A. Schadschneider, and A. Seyfried, *Universal flow-density relation of single-file bicycle, pedestrian and car motion*, Phys. Lett. A, 378 (2014), pp. 3274–3277.